Construction and Building Materials 348 (2022) 128692

Contents lists available at ScienceDirect

Construction and Building Materials

journal homepage: www.elsevier.com/locate/conbuildmat

Crack width control and mechanical properties of low carbon engineered cementitious composites (ECC)

Mengjun Hou, Duo Zhang, Victor C. Li *

Department of Civil and Environmental Engineering, University of Michigan, Ann Arbor, MI, USA

ARTICLE INFO

Keywords:
Engineered Cementitious Composites (ECC)
Limestone Calcined Clay Cement (LC3)
Polypropylene (PP) fiber
Crumb rubber
Crack width control

ABSTRACT

Engineered Cementitious Composites (ECC) have superior properties with high tensile ductility and tight crack width compared to conventional concrete. The properties of ECC are significantly influenced by the material composition which can be tailored to enhance the sustainability of ECC. Towards this goal, recycled crumb rubber (CR) and silica fume (SF) were used to tailor the properties of a polypropylene-fiber reinforced ECC with a low carbon binder based on limestone calcined clay cement (LC3) in this study. Crumb rubber was found to be effective in enhancing strain-hardening performance and reducing the width of the multiple microcracks. However, a loss of compressive strength was accompanied by an increasing amount of CR. While silica fume or lower w/b ratio enhanced the compressive strength, the crack width of ECC increased at higher SF content or lower w/b. The underlying mechanisms of these trends were traced to the alteration of the matrix fracture toughness and fiber/matrix interfacial bond. Rubber particle bridging was found to contribute to crack width control. The combined use of the LC3 green binder and CR led to a lowering of the embodied and operational carbon footprint of ECC.

1. Introduction

Engineered Cementitious Composite (ECC) has been studied in the past decades and has proven superior mechanical and durability properties. Compared to conventional concrete which fails in a brittle manner, ECC has tensile ductility of at least 2 %, 200 times that of conventional concrete. In addition, ECC exhibits multiple cracking behaviors during the strain-hardening stage [1]. The mechanical properties of ECC depend on three factors: fiber, matrix, and fiber/matrix interface, the individual properties of which can be tailored for the robust strain-hardening performance based on the micromechanics model [2].

In terms of fiber types, PVA fiber is widely used in traditional ECC with excellent ductility and durability of infrastructures [3–6], while the production of PVA fiber involves large energy consumption, carbon emissions and cost, which is responsible for the high economic and environmental impacts of ECC. This recognition has prompted the search of greener and lower-cost fiber options. For example, high tenacity Polypropylene (HTPP) fiber was studied in [7–10]. Although PP ECC has ductility comparable to PVA ECC, its crack control ability is weaker due to relatively lower fiber modulus and fiber/matrix interfacial properties. The average crack width under tension is in the range of 80–150 μm [8,9], much larger than that of PVA ECC (50–100 μm) [1]. The larger crack width diminishes the durability of PP ECC.

The binder composition of ECC contributes to both the mechanical properties and the greenness of ECC [11,12]. Fly ash (FA) is the most widely used supplementary cementitious materials (SCMs) in ECC design. Fly ash has advantages beyond reducing the embodied carbon of ECC, including its contribution to long-term strength gain due to its pozzolanic activity, enhancement in workability, and reduction in the heat of hydration and drying shrinkage. The averaged crack width is reduced and the robustness of ECC tensile ductility is enhanced [13–16]. Nevertheless, the physical and chemical properties of FA significantly depend on the power plant and the coal type, resulting in the variability of composite properties. Tosun-Felekoglu et al. [10] found that the physical and chemical properties of fly ash directly affect the performance of composites both in fresh and hardened states. F-type fly ash was more advantageous in producing HTPP-ECC compared to C-type fly ash employed in that study. Ma et al. [17] found that the fly ash with relatively higher calcium content and smaller particle size was conducive to a higher compressive strength. The lower combined Al_2O_3 and CaO content of this fly ash enhanced the tensile strain capacity.

* Corresponding author.
E-mail address: vcli@umich.edu (V.C. Li).

https://doi.org/10.1016/j.conbuildmat.2022.128692
Received 9 June 2022; Received in revised form 1 August 2022; Accepted 3 August 2022
Available online 8 August 2022

Table 1
Mixture proportion (by weight) of ECC (with 2 vol% PP).

Variable	Mixture	OPC	MK	LM	FA	CR[a]	SF[b]	Water	w/b	SP
CR	M−CR0	1	0.5	0.5	2	–	–	1	0.25	0.013
	M−CR10	1	0.5	0.5	1.8	10 %	–	1	0.25	0.013
	M−CR30	1	0.5	0.5	1.4	30 %	–	1	0.25	0.013
	M−CR50	1	0.5	0.5	1	50 %	–	1	0.25	0.013
	M−CR70	1	0.5	0.5	0.6	70 %	–	1	0.25	0.013
	M−CR100	1	0.5	0.5	0	100 %	–	1	0.25	0.013
SF	M−CR50−SF5	0.95	0.5	0.5	1	50 %	5 %	1	0.25	0.013
	M−CR50−SF10	0.9	0.5	0.5	1	50 %	10 %	1	0.25	0.013
	M−CR50−SF15	0.85	0.5	0.5	1	50 %	15 %	1	0.25	0.013
	M−CR50−SF20	0.8	0.5	0.5	1	50 %	20 %	1	0.25	0.013
w/b	M−CR50−SF20−0.20	0.8	0.5	0.5	1	50 %	20 %	0.8	0.20	0.018
	M−CR50−SF20−0.15	0.8	0.5	0.5	1	50 %	20 %	0.6	0.15	0.031

[a] Substitution ratio of fly ash with crumb rubber by volume.
[b] Substitution ratio of cement with silica fume by mass.

Furthermore, high calcium fly ash accelerates the self-healing process of ECC for the same pre-damaged level. Kan et al. [18] reported that the reactivity of fly ash is the determining factor for ECC's compression performance. Fly ash with a higher calcium content did not lead to higher tensile properties at all ages but did consistently enhance the compressive performance.

In recent years, a new type of binder, calcined clay limestone cement (LC3), where a high level of clinker is substituted by a combination of calcined clay and limestone, has gained interest due to its greenness potential and wide availability of raw materials [19]. Researchers have utilized LC3 binder in ECC composite and found the resultant advantages in the mechanical performance of ECC, such as early strength enhancements [20], higher tensile strain capacity [21], and improved flexural strength [22]. In addition, silica fume, another alternative SCM that is used in this study, also improves the mechanical properties and durability of ECC. Silica fume was proven to enhance the strength of ECC due to its strong pozzolanic reactivity and nano-sized particle size [11,23], and the durability of ECC as well [24].

The preliminary experiment for this study shows that the fly ash used in this study results in a higher first cracking strength due to the ultra-fineness of fly ash particles which leads to a higher matrix fracture toughness. The excessively high cracking stress is not beneficial for meeting the strength criterion ($\sigma_0/\sigma_{fc} \geq 2$) of pseudo-strain-hardening [7,25]. The strategy for tailoring the properties of ECC as suggested in [26] is adopted in the following work.

The introduction of artificial flaws is an effective way to counteract the tendency of rising fracture toughness. The particles with low strength or weak bonds to the cementitious matrix are preferred as artificial flaws, such as polystyrene beads, fly ash cenosphere, entrained air, vermiculite, crumb rubber, etc [23,26–29]. Specifically, crumb rubber as an industrial waste can be used to enhance the properties of ECC and minimize the embodied carbon of ECC [30]. Crumb rubber has been used to replace silica sand or fly ash as an inert filler in ECC composition. The relevant research shows that crumb rubber can reduce the composite density, improve tensile ductility [23,29,31–34], and improve other durability properties [34] and impact resistance [35]. However, a reduction in compressive strength is observed by the addition of crumb rubber in these research works. To counteract this tendency, the incorporation of silica fume as commonly used in enhancing the compression strength of conventional concrete [36,37] is considered.

The objective of this study is to develop an LC3-based PP-ECC with lower embodied and operational energy and carbon footprint than traditional PVA-ECC, and with good crack width control. Specifically, the hypothesis that the mechanical properties and tight crack width of PP-ECC can be tailored by a combination of crumb rubber, silica fume, and low water/binder ratio is experimentally tested. Crumb rubber and silica fume replaced fly ash and cement in the mixture composition, respectively. The impact of these variables on the matrix fracture toughness, fiber/matrix interface bonding, mechanical properties of ECC and crack width control were investigated. The mechanism of crack width control was discussed, and the environmental and economic impacts were analyzed accordingly. The research findings provide a deeper understanding of crack width control of ECC and have the potential to improve the durability of ECC under various environmental exposures. This in turn leads to lower operational carbon due to reduced maintenance needs in the use phase of infrastructures. In this manner, this study represents a novel approach to simultaneously lower the embodied and operational carbon of civil infrastructure built with ECC.

Table 2
Chemical composition of fly ash and silica fume (%).

	SiO_2	Al_2O_3	Fe_2O_3	SO_3	CaO	MgO	K_2O
FA	51.6	16.2	5.0	1.4	10.8	3.7	2.5
SF	96.5	0.7	0.3	0.5	0.4	0.5	0.85

Table 3
Physical properties of PP fiber.

Diameter/ μm	Length/ mm	Strength/ MPa	Elastic modulus/ GPa	Elongation/ %	Density/ (g/cm^3)
12	12	910	9	22	0.91

2. Experimental studies

2.1. Mix design and materials

Table 1 shows the mixture composition of ECC. The LC3 binder is composed of type I ordinary Portland cement (OPC) from Argos, metakaolin (MK) and limestone (LM) provided by Imerys. The chemical compositions of ASTM Class F fly ash (FA) from Boral and silica fume (SF) provided by Elkem are shown in Table 2. The physical properties of Polypropylene (PP) fiber provided by Saint-Gobain are shown in Table 3. Crumb rubber is provided by Michelin Tires with an average particle size of 51 μm and a bulk density of 0.43 g/cm^3. The SEM images of fly ash and crumb rubber are shown in Fig. 1. The superplasticizer (SP) from BASF (MasterGlenium 7920) was used for water reduction.

A series of experiments were conducted to determine the mechanical properties and the crack width of ECC. The mixture proportions are listed in Table 1 with variations in crumb rubber (CR) content, silica fume (SF) content, and water/binder ratio(w/b). CR substituted FA by volume in the range of 10 % to 100 %. Silica fume substituted cement by mass from 5 % to 20 %. Three water/binder ratios (0.25, 0.20, 0.15) were also investigated. The content of SP was varied based on the fresh properties of the matrix.

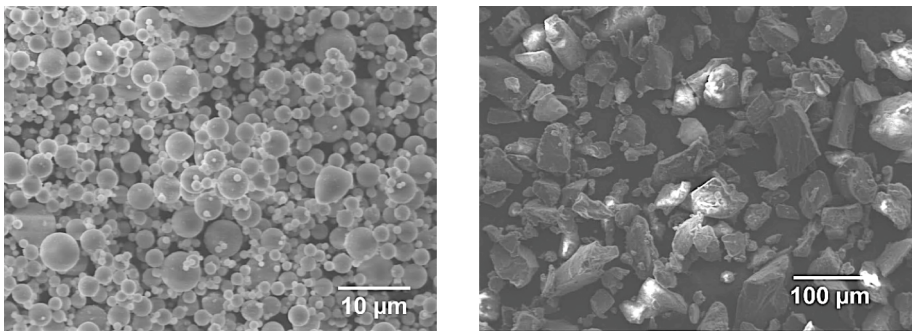

(a) Fly ash (b) Crumb rubber

Fig. 1. SEM images of fly ash and crumb rubber.

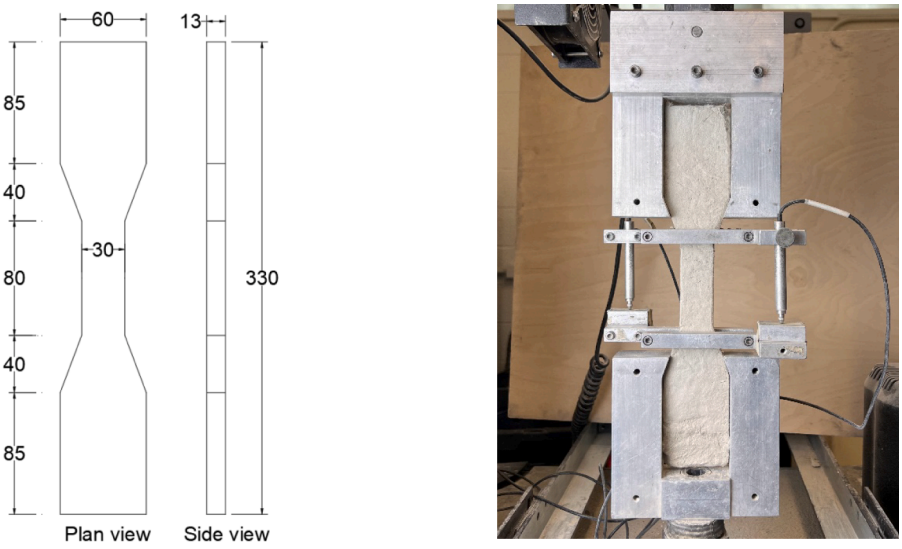

(a) Specimen dimensions (b) Test set-up

Fig. 2. Dogbone-shaped specimen and test set-up for uniaxial tension test(unit: mm).

2.2. Specimen preparation

Fiber dispersion is related to mixer type, mixing force/speed, mixing time, and optimal viscosity of the matrix [9,38]. To obtain proper fiber dispersion, the mixing speed and time were experimentally optimized in this study. Specifically, all mixtures were prepared with an 18-liter Hobart mixer. Dry ingredients without fiber were first mixed at a low speed for 5 min to ensure sufficient blending. Then water and superplasticizer were added and mixed for another 5 min at a medium speed to obtain a uniform fresh mortar. Fibers were subsequently added slowly and mixed for 7–8 min to achieve a uniform fiber distribution. Afterward, the fresh ECCs were cast into cube molds (50 × 50 × 50 mm^3) and the dogbone-shaped molds with the geometry recommended by the Japan Society of Civil Engineers (JSCE) [39] (Fig. 2(a)) for compressive test and uniaxial tension test, respectively. All specimens were de-molded after 24 h, and then cured till the testing age of 28 days.

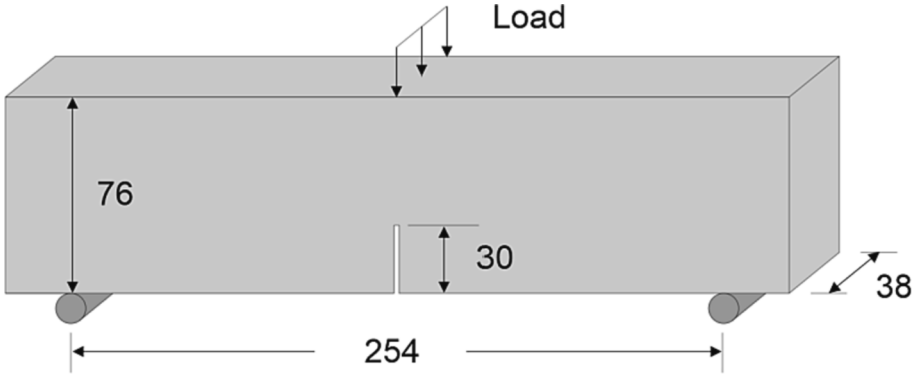

Fig. 3. Three-point bending test set-up (unit: mm).

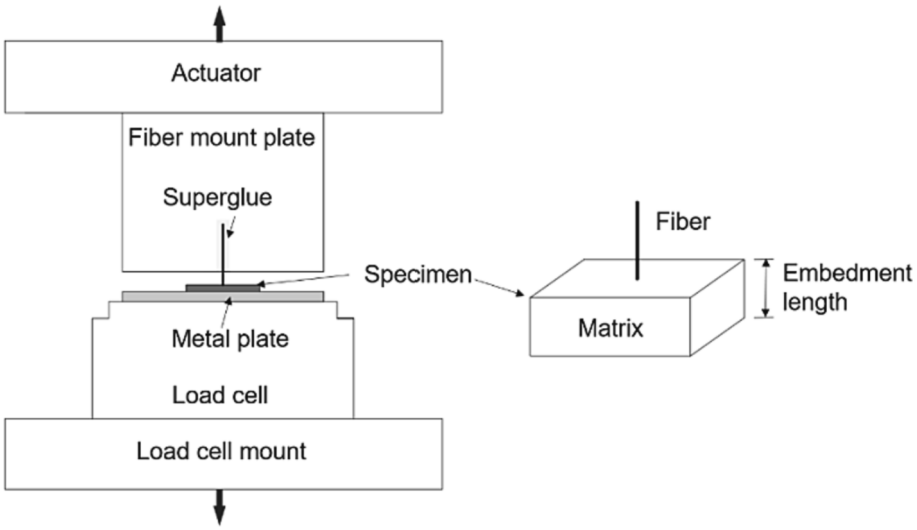

Fig. 4. Single-fiber pullout test set-up.

The curing condition has an impact on the mechanical properties of ECC, while the gap of mechanical properties between various humidity curing narrow with age [40]. In this study, air curing was chosen for all specimens.

The matrix beam specimens ($38 \times 76 \times 305$ mm^3) were prepared for matrix fracture toughness measurement using the same mixing procedure except for fiber addition. The single fiber pullout test samples were prepared following the procedure described in [41,42]. A long PP fiber was embedded in the ECC matrix. The hardened specimens were cut into small platelets using a diamond precision saw with an embedment length before testing.

2.3. Testing procedure

The compressive test was conducted with cube specimens at a loading rate of 0.5 MPa/s in accordance with ASTM C109 [43]. The uniaxial tension test was carried out on the dogbone-shaped specimens using an Instron servo-hydraulic system with a displacement control rate of 0.5 mm/min as recommended by JSCE[39]. Two external linear variable displacement transducers (LVDT) with a gauge length of 80 mm were attached to the middle part of the specimen for deformation recording (Fig. 2(b)). The tensile stress–strain relationship was determined accordingly. The first crack strength, ultimate tensile strength,

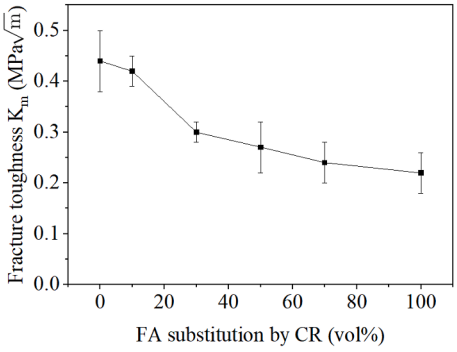

(a) Fracture toughness with varying CR content

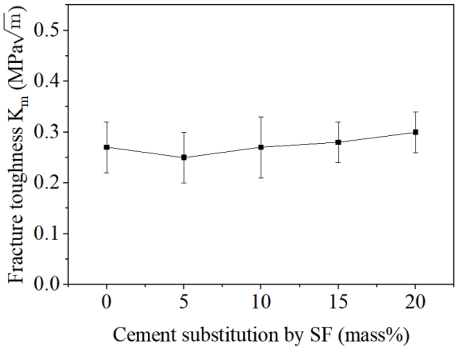

(b) Fracture toughness with varying SF content with 50% CR content

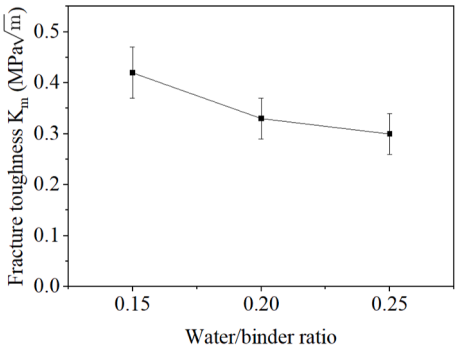

(c) Fracture toughness with varying w/b ratio with 50% CR content and 20% SF content

Fig. 5. Influence of CR, SF and water/binder ratio on matrix fracture toughness.

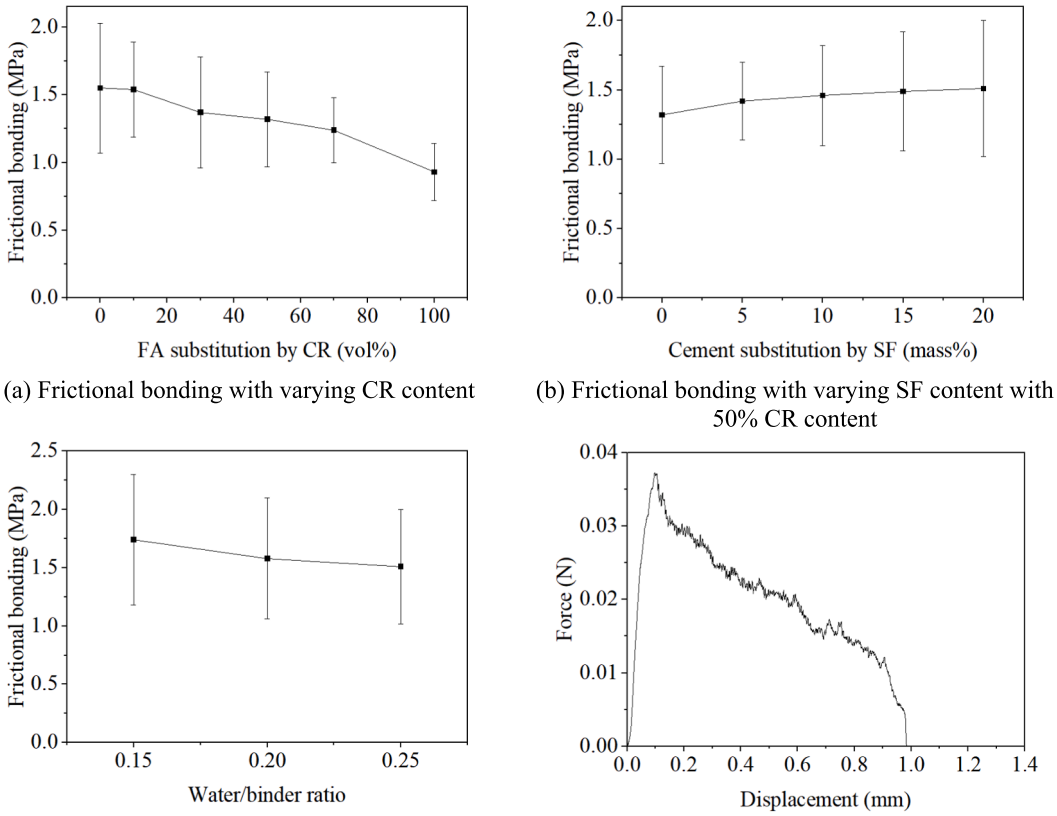

(a) Frictional bonding with varying CR content

(b) Frictional bonding with varying SF content with 50% CR content

(c) Frictional bonding with varying w/b ratio with 50% CR content and 20% SF content

(d) Pullout behavior of single PP fiber

Fig. 6. Influence of CR, SF and water/binder ratio on interfacial bonding and the pullout behavior of PP fiber.

and tensile strain capacity were extracted from the tensile stress–strain relations. During the loading process, the crack number was recorded at one percent strain increment to calculate the corresponding average crack width. The details are discussed in the following section.

The matrix fracture toughness was determined by the three-point bending test following ASTM E399 [44]. As shown in Fig. 3, the beam specimen was pre-notched with a diamond cutting saw and supported with a span of 254 mm. The bending test was conducted under the displacement control rate of 0.02 mm/min. Due to the absence of coarse aggregate in ECC mixture, the fracture process zone size is small compared to the relevant laboratory specimen dimensions. Thus it is reliable to determine fracture toughness by the linear elastic fracture mechanics (LEFM) method [45]. The fracture toughness K_m can be calculated by the following equations.

$$K_m = \frac{PS}{BW^{1.5}} \bullet f\left(\frac{a}{W}\right) \tag{1}$$

$$f\left(\frac{a}{W}\right) = 3\sqrt{\frac{a}{W}} \bullet \frac{1.99 - \left(\frac{a}{W}\right)\left(1 - \frac{a}{W}\right)\left[2.15 - 3.93\frac{a}{W} + 2.7\left(\frac{a}{W}\right)^2\right]}{2\left(1 + 2\frac{a}{W}\right)\left(1 - \frac{a}{W}\right)^{1.5}} \tag{2}$$

where P is the maximum load; S is the span of the beam; B is the width of the beam; W is the specimen height; a is the notch depth.

Single-fiber pullout test was conducted to obtain the interfacial fiber/matrix bonding [41,42]. As shown in Fig. 4, the specimen bottom was glued onto a metal plate attached to a high-precision load cell (±10 N range) and the free end of PP fiber was glued to another plate clamped to an actuator. The fiber is pulled out at a displacement rate of 0.2 mm/min. The embedment length was controlled between 0.7 mm and 1.3 mm. At least 10 specimens were tested for each mixture. It was found that the chemical bonding is negligible due to the hydrophobicity of PP fiber. The frictional bonding can be calculated by the following equation.

$$\tau_0 = \frac{P_d}{\pi d_f L_e} \tag{3}$$

where τ_0 is the frictional bond; P_d is the maximum load; d_f is the diameter of fiber; and L_e is the embedment length.

3. Results and discussion

3.1. Matrix fracture toughness

The matrix fracture toughness of all mixtures is shown in Fig. 5. The data in Fig. 5 (a) indicate that the fracture toughness of the matrix is reduced with increasing crumb rubber content. When fly ash is fully replaced by crumb rubber, the fracture toughness is reduced by around 50 %. Crumb rubber is hydrophobic and weakly bonded to the surrounding matrix [46]. The cement hydration near rubber particles was hindered and a clear interface between matrix and rubber particles can be observed via SEM [47]. Since the crumb rubber is inert while fly ash undergoes a pozzolanic reaction process, the energy associated with breaking material bonds at the crack tip may be expected to be reduced, consistent with a lowering of fracture energy and K_m when fly ash is replaced by crumb rubber.

Fig. 5 (b) shows the effect of silica fume on matrix fracture toughness. The fracture toughness shows a slight reduction when 5 % of cement is replaced by silica fume, followed by a gradual increase with increasing SF content up to 11.1 % compared to the non-SF matrix. This can be attributed to the fact that silica fume promotes the formation of hydration products as a highly effective pozzolanic material in addition

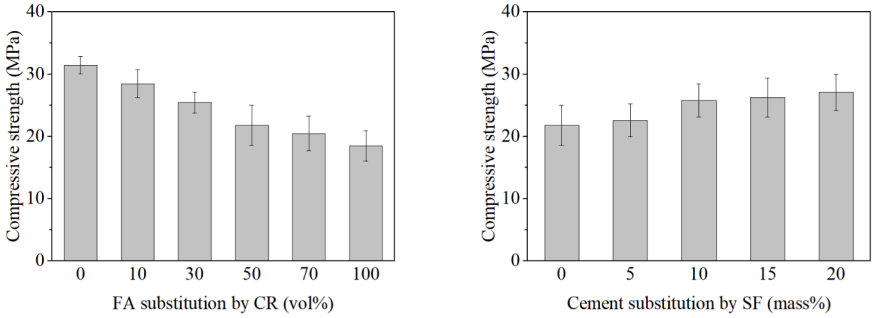

(a) Compressive strength with varying CR content

(b) Compressive strength with varying SF content with 50% CR content

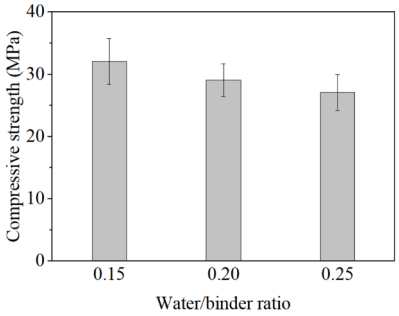

(c) Compressive strength with varying w/b ratio with 50% CR content and 20% SF content

Fig. 7. Influence of CR, SF and water/binder ratio on compressive strength.

to matrix densification by virtue of its small particle size [48]. The observed variations in K_m, however, are within the data noise range.

The increase in the w/b ratio from 0.15 to 0.25 leads to a significant drop in K_m from 0.42 MPa$\sqrt{m}$ to 0.30 MPa$\sqrt{m}$, as shown in Fig. 5 (c). It should be noted that during the material processing, the amount of superplasticizer was adjusted for better flowability of fresh mortar to ensure good fiber dispersion (Table 1), and more SP was required at low w/b ratios. This might introduce some influence on the microstructure of the matrix and further on the fracture properties. Nevertheless, decreasing the w/b ratio has a densification effect on the matrix microstructure, resulting in a compact matrix with fewer defects, consistent with what has been reported in the literature [49,50].

3.2. Fiber/matrix interfacial properties

Fig. 6 shows the influence of CR, SF and w/b ratio on interfacial bonding. Due to the hydrophobicity of PP fiber, the chemical bonding is negligible between the matrix and PP fiber, and the typical pullout load–displacement curve in this study is shown in Fig. 6(d). As shown in Fig. 6(a), the friction bonding τ_0 is reduced with crumb rubber content. Crumb rubber is inert and has no chemical reaction with the cementitious matrix. Due to this chemical incompatibility, the addition of crumb rubber changed the microstructure of the interface transition zone (ITZ) both chemically and physically, with fewer hydration products and increased porosity, thus leading to the observed reduction of frictional bonding of fiber/matrix [31].

Silica fume shows an increasing impact on the interfacial bonding of fiber/matrix as shown in Fig. 6(b). The frictional bonding is increased by 14.4 % when 20 mass% of cement is replaced by silica fume, which stems from the densification of ITZ by the pore-size refinement effect of silica fume. Decreasing the w/b ratio has a similar effect on the interfacial bonding of fiber/matrix (Fig. 6(c)). As discussed in Section 3.1, reducing the water amount in the mixture can densify the matrix as well as ITZ, which provides more frictional resistance for fiber pullout behavior. It should be noted that the measured interfacial bonding has a relatively high variability due to the sensitivity of the single-fiber pullout test and the small size of samples, consistent with that reported in the literature [31,51–53].

3.3. Mechanical properties of ECC

3.3.1. Compressive strength

Fig. 7 shows the relationship between compressive strength and mixture composition variables. As seen in Fig. 7(a), the compressive strength decreases gradually with crumb rubber content. When fly ash is substituted by crumb rubber at 50 vol% and 100 vol%, the compressive strength is reduced by 30.7 % and 41.2 %, respectively. This can be attributed to the low strength and modulus of crumb rubber partially. On the other hand, the incompatibility of rubber particles in the matrix leads to the weak bond between crumb rubber and the cementitious matrix. Viewed in this manner, crumb rubber may serve as artificial defect sites that lower the compressive strength of the composite.

The effect of silica fume on the compressive strength is similar to that of fracture toughness as shown in Fig. 7(b). Due to the highly pozzolanic activity, the hydration products accumulate in the matrix even with the decreased cement content. In addition, the fine particles of silica fume are expected to fill the voids and refine the matrix microstructure. Thus, when 20 mass% of cement is replaced by silica fume, the compressive strength is increased to 27.1 MPa, which is close to that of M−CR10.

Similarly, lowering the amount of water in the mixture led to an increase in compressive strength as expected. When the w/b ratio is reduced from 0.25 to 0.15, the compressive strength is increased by 18.3 % to 32.1 MPa, which is comparable to that of the control mixture M−CR0.

3.3.2. Tensile properties

The tensile stress–strain curves of ECC with different CR contents are shown in Fig. 8. The crack pattern picture at the last percent strain of each mixture was also included, e.g., the crack pattern picture is attached at 3 % tensile strain for M−CR0 with the ultimate tensile strain

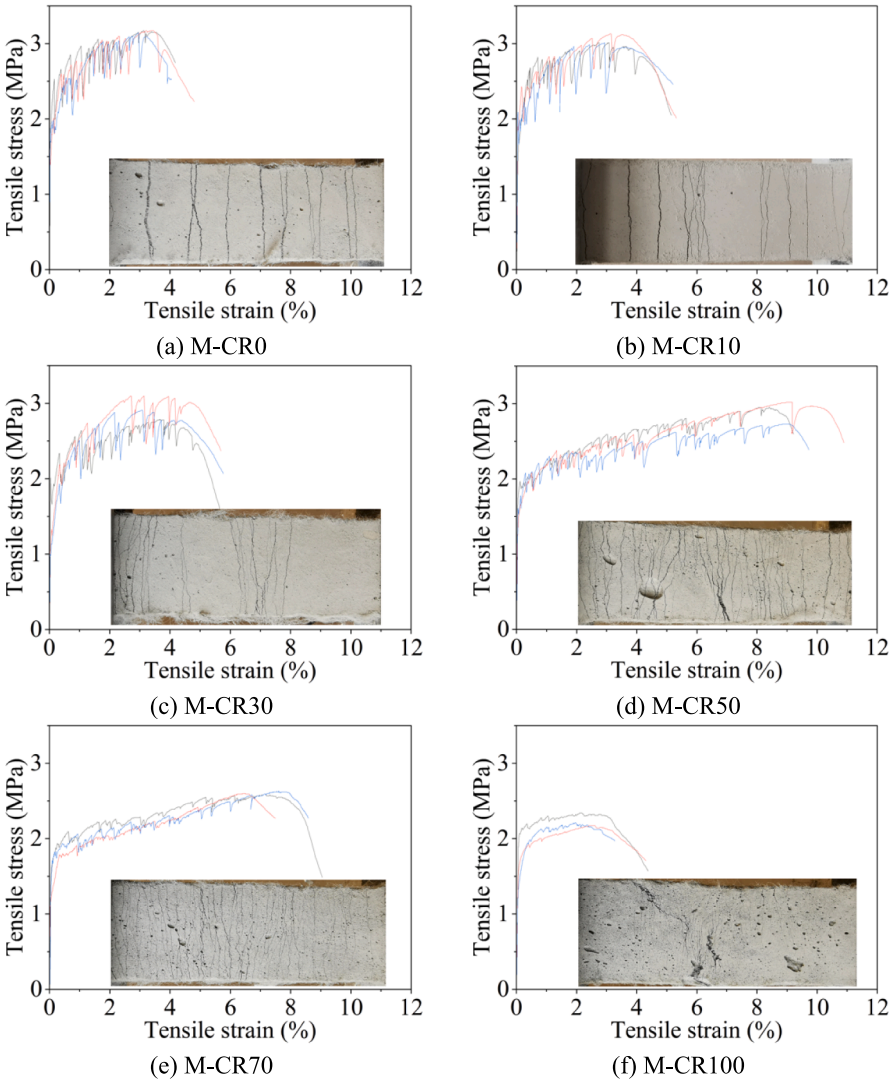

Fig. 8. Tensile stress–strain curves with CR contents and corresponding crack pattern at the last strain percent.

Table 4
Summary of tensile properties of all ECC mixtures at 28 days.

Mixture	First cracking strength σ_{fc} (MPa)	Ultimate tensile strength σ_{ut} (MPa)	Tensile strain capacity ε_{ut}	Crack number	Average crack spacing(mm)
M−CR0	1.91 ± 0.02	3.16 ± 0.01	3.37 %±0.20 %	16 ± 1	5.04 ± 0.42
M−CR10	1.86 ± 0.15	3.05 ± 0.06	3.42 %±0.39 %	17 ± 2	4.85 ± 0.47
M−CR30	1.72 ± 0.33	2.93 ± 0.13	3.83 %±0.27 %	23 ± 7	3.71 ± 0.95
M−CR50	1.65 ± 0.12	2.90 ± 0.12	8.61 %±0.41 %	58 ± 3	1.37 ± 0.07
M−CR70	1.55 ± 0.18	2.61 ± 0.02	7.01 %±0.48 %	70 ± 4	1.15 ± 0.07
M−CR100	1.52 ± 0.24	2.24 ± 0.07	2.42 %±0.38 %	53 ± 12	1.60 ± 0.35
M−CR50−SF5	1.67 ± 0.09	3.20 ± 0.07	10.39 %±0.35 %	74 ± 3	1.08 ± 0.04
M−CR50−SF10	1.68 ± 0.23	2.83 ± 0.04	5.68 %±0.08 %	41 ± 8	2.04 ± 0.37
M−CR50−SF15	1.79 ± 0.10	3.09 ± 0.09	5.50 %±0.47 %	36 ± 3	2.22 ± 0.20
M−CR50−SF20	1.97 ± 0.11	3.21 ± 0.09	4.55 %±0.48 %	31 ± 2	2.60 ± 0.21
M−CR50−SF20−0.20	2.09 ± 0.02	3.51 ± 0.04	4.92 %±0.35 %	33 ± 2	2.41 ± 0.19
M−CR50−SF20−0.15	3.10 ± 0.29	3.82 ± 0.07	2.98 %±0.82 %	14 ± 2	5.77 ± 1.09

capacity of 3.37 %, etc. The tensile performance of all the mixtures is summarized in Table 4 and shown in Fig. 10. The average crack spacing was calculated based on the crack number of the 80 mm center region of the sample.

It can be seen that the cracking stress is related to the CR content. Specifically, the first cracking strength was gradually decreased from 1.91 MPa to 1.52 MPa as CR substituted FA from 0 vol% to 100 vol%. This can be attributed to the weakened matrix fracture toughness caused by crumb rubber as discussed in Section 3.1. The hydrophobicity of crumb rubber leads to the weak interfacial zone between cementitious matrix and rubber particles, and microcracks are activated from these low-bonded areas as well as other microstructure flaws or defects (e.g. voids). In other words, the existence of crumb rubber in the ECC matrix can be seen as an artificial flaw even though the rubber particles have a small average size (51 μm in this study).

The improved flaw distribution by crumb rubber ensures saturated

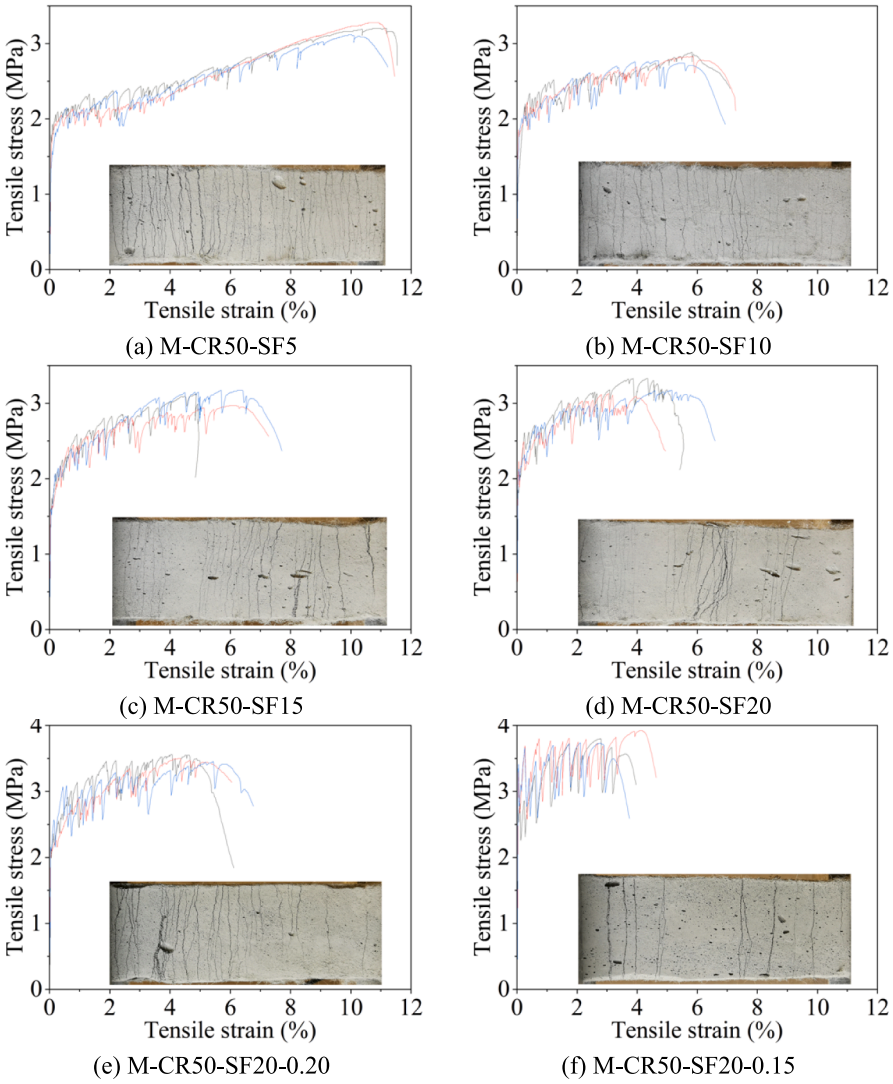

Fig. 9. Tensile stress–strain curves of ECC with SF contents or w/b ratios and corresponding crack pattern at the last strain percent.

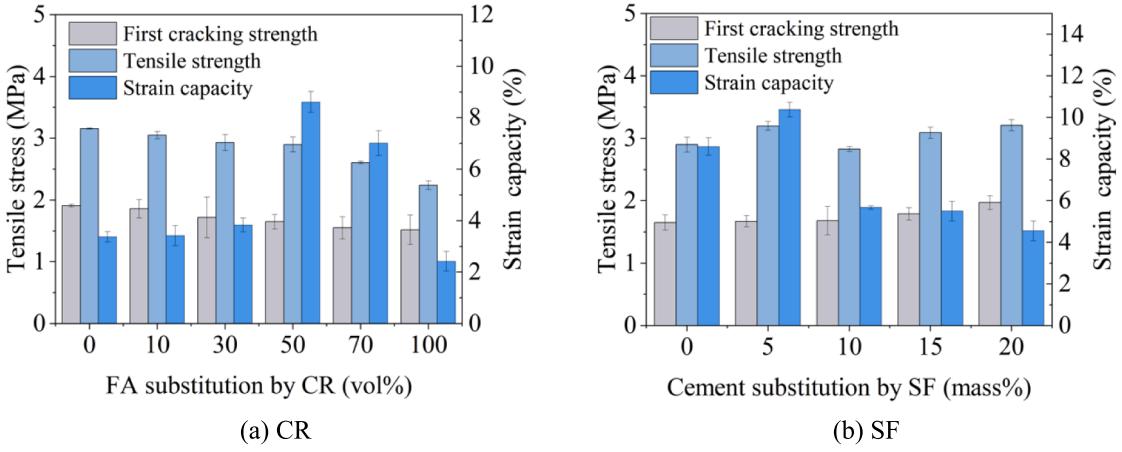

Fig. 10. Tensile performance of ECC mixtures with CR and SF contents.

multiple cracking, which is responsible for the cumulative inelastic deformation in the strain-hardening stage. The crack number increased with CR content and reached a peak at 70 % CR content with the lowest crack spacing of 1.15 mm and the tensile strain capacity of 7.01 % (M−CR70). However, M−CR50 exhibits a better tensile strain capacity (8.61 %) with less crack number than that of M−CR70, which suggests a larger crack width as shown in Fig. 8(d).

The tensile strength exhibits a similar decreasing trend as the first

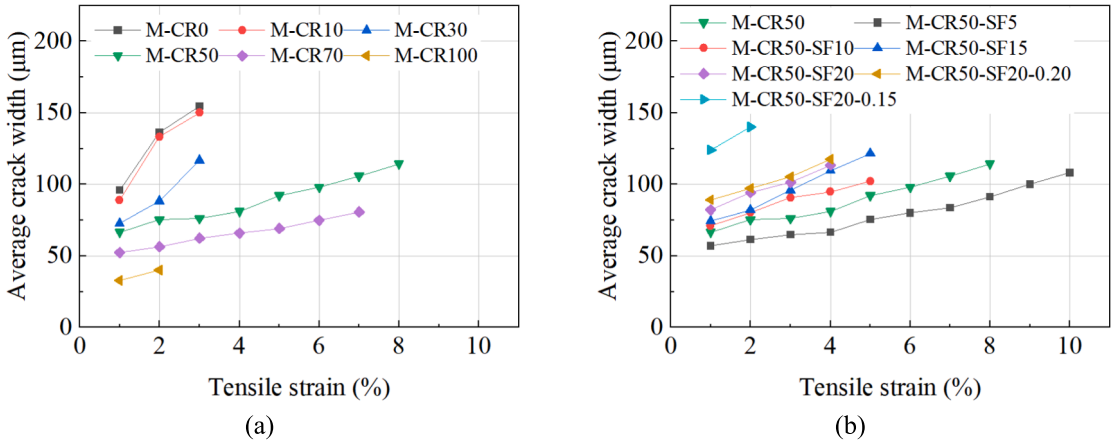

Fig. 11. Evolution of average crack width with tensile strain as influenced by (a) crumb rubber, and (b) silica fume and w/b ratio.

cracking strength with CR content, which results from the reduced fiber bridging capacity. The fiber bridging capacity is related to fiber strength, fiber content, and interfacial bonding. Crumb rubber caused a less compact interface transition zone and reduced frictional bonding of fiber/matrix (Fig. 6(a)), resulting in reduced fiber bridging capacity. It should be noted that for M−CR100, the low fiber bridging capacity is not only attributed to a low interfacial bonding of fiber/matrix but also to the less uniform fiber dispersion. When fly ash was replaced by crumb rubber completely, the mixing difficulty negatively impacted the fiber dispersion. Even with these impacts, M−CR100 exhibits the saturated multiple cracking with tight crack width as shown in Fig. 8(f).

Fig. 9 shows the tensile stress–strain curves of mixtures with increasing silica fume content and lowering water/binder ratio, respectively. As shown in Table 4 and Fig. 10(b), the first cracking strength is increased progressively from 1.65 MPa to 1.97 MPa with silica fume substituting cement in the range of 0 %-20 %. This is related

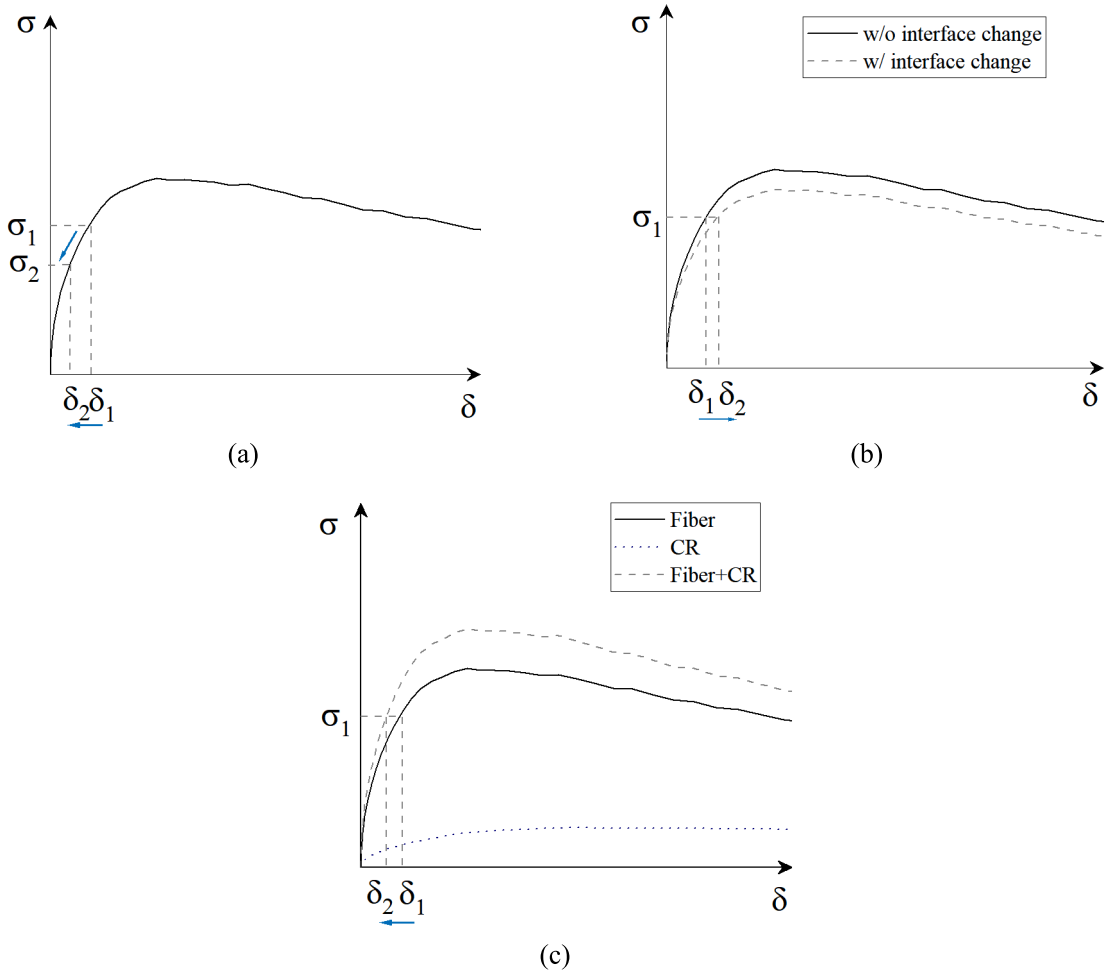

Fig. 12. The effects of crumb rubber on σ-δ relationship in terms of (a) weakened matrix; (b) interfacial bonding change; (c) CR particle bridging.

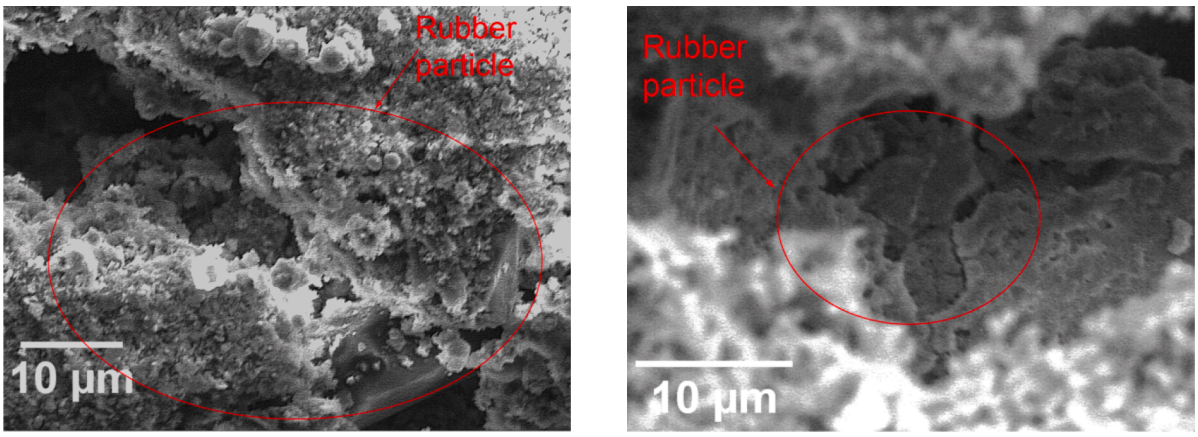

Fig. 13. SEM images: Rubber particles bridging the crack faces.

to the increased matrix fracture toughness caused by the highly pozzolanic reactivity and ultra fineness of silica fume to densify the cementitious matrix microstructure as discussed in Section 3.1. The resultant densification of the interfacial transition zone increases the frictional bonding of PP/matrix (Fig. 6(b)), leading to the enhancement of fiber bridging capacity. Specifically, when silica fume replaced cement at 5 % (M−CR50−SF5), the first cracking strength remains at almost the same level as the non-SF mixture (M−CR50). However, with increased frictional bonding, the fiber bridging capacity and tensile strength are enhanced, i.e., the tensile strength and strain capacity of M−CR50−SF5 increased by 10.3 % and 20.7 % over that of M−CR50, respectively. With further increasing SF content, the densification of the matrix leads to higher cracking stress, which is not beneficial for multiple cracking, resulting in lowered crack numbers and tensile strain capacity.

Similarly, lowering the w/b ratio further densified the matrix microstructure with reduced porosity, and led to increasing cracking stress and tensile strength. When the w/b ratio is reduced to 0.20, the first cracking strength and ultimate tensile strength are increased to 2.09 MPa and 3.51 MPa, respectively. Although the tensile strain capacity and the ultimate crack number are increased, from the tensile stress–strain curve (Fig. 9(e)), there is a larger fluctuation in the strain-hardening stage, indicating a larger crack width compared to that of the w/b ratio at 0.25 (M−CR50−SF20). Likewise, the lowest w/b ratio (0.15) led to the largest cracking stress and tensile strength, but unsaturated multiple cracking and the largest crack width (Fig. 9(f)).

3.3.3. Crack pattern

The evolution of average crack width with tensile strain is shown in Fig. 11. As expected, the crack width increased with increasing tensile strain for all mixtures. As shown in Fig. 11(a), the average crack width at the same tensile strain decreased with increasing CR content. For example, at 1 % tensile strain, the crack width decreases by 7.4 % to 65.8 % as CR content increases from 10 % to 100 % replacement of FA.

At small CR content (less than 30 %), it is observed that the average crack width increased at a steep rate with tensile strain, nearly the same as that of non-CR ECC (M−CR0). This is consistent with the tensile stress–strain curves as shown in Fig. 8(a)-(c), where the tensile strain performance did not exhibit obvious improvement with large fluctuation in the strain-hardening stage. With increasing CR content over 30 %, the crack width vs strain curve slope is gentler, consistent with the lessened fluctuations in the tensile stress–strain curves as shown in Fig. 8 (d)-(f). For M−CR100, the tensile stress–strain curve is nearly smooth, with a tight crack width of 40 μm at 2 % tensile strain and intensive multiple cracks as shown in Fig. 8(f). As discussed previously, the improved flaw distribution by crumb rubber triggers more microcracks at lower stress even though the weakened frictional bonding of fiber/matrix tends to enlarge fiber slippage and crack opening.

As shown in Fig. 11(b), the crack width is reduced at a low SF content of 5 % (M−CR50−SF5) compared to that of non-SF ECC (M−CR50). As discussed in Section 3.3.2, the cracking stress did not reveal an obvious increase, but with an increased frictional bonding, the fiber slippage at the same cracking stress is lowered, resulting in the reduction of crack width, which is reflected in the fluctuations of the tensile stress–strain curve in Fig. 9(a). However, with further increasing SF content, a more densified matrix leads to higher cracking stress, so larger fluctuations in the tensile stress–strain curve and fewer crack numbers are observed in Fig. 9(b)-(d). Similarly, lowering the w/b ratio further densified the matrix, leading to a higher cracking stress with large stress fluctuations. Especially for the w/b ratio of 0.15 (M−CR50−SF20−0.15), the first cracking strength reached 3.10 MPa with the highest stress fluctuation up to 0.9 MPa, and accompanied by an average crack width of 124 μm and 140 μm at 1 % and 2 % tensile strain, respectively.

3.4. Mechanism of crack width control

The potential mechanisms behind crack width control by crumb rubber are illustrated in Fig. 12, where σ_1 and σ_2 represent the cracking stress and δ_1 and δ_2 represent the corresponding crack opening. The subscript "1″ indicates the original value of the parameter, and the subscript "2" indicates the changed value of the parameter as a result of the suggested crack-width-reduction mechanism. Firstly, the introduction of CR to the matrix composition leads to weak bonding of CR/matrix as well as decreased cracking stress. In terms of the stress-crack opening (σ-δ) relation as shown in Fig. 12(a), the crack opening is positively related to the stress in the ascending branch. The lowered cracking stress leads to the reduction of crack width, which is supported by established literature [27,28]. However, as discussed in Section 3.2, the change in the microstructure of the fiber/matrix interface induced by CR leads to a weakened fiber/matrix interfacial bond. This is not beneficial for crack width control. The slope of the σ-δ curve is associated with fiber stiffness and volume fraction, as well as the interfacial bonding of fiber/matrix. As shown in Fig. 12(b), a weakened interfacial bond reduces the slope of the σ-δ curve, resulting in a larger crack width for a given stress level [9,13]. A third plausible mechanism of crack width control is bridging of microcracks by CR particles, on top of bridging provided by fibers. As shown in Fig. 13, the cracking region of tensile specimens after the tension test was observed via SEM. CR particles were found to link the crack faces even though the crack was fully formed in the cross-section. Due to the irregular shape and low elastic modulus of CR particles, some particles could be interlocked in the

Table 5
Cost, embodied energy, and CO_2 emission of ECC ingredients.

	OPC[a]	LC3[a]	FA[b]	CR[c]	SF[b]	Water	SP[d]	PP[e]	PVA[f]
Embodied energy (GJ/ton)	5.15	4	0	4	0	0	35	77	101
CO2 emission(kg/ton)	970	560	0	200	0	0	1667	3100	3400
Cost ($/ton)	72.02	56.41	26.5	320	300	1.5	1211	6335	12,670

[a] Data from [12,55].
[b] Data from the local market price.
[c] Data from [57,58].
[d] Data from [59].
[e] Data from [21,60].
[f] Data from [20,21,60].

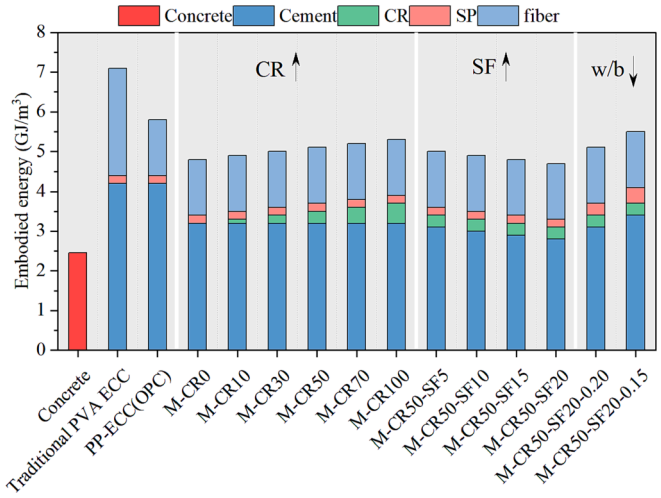

Fig. 14. Embodied energy of all mixtures.

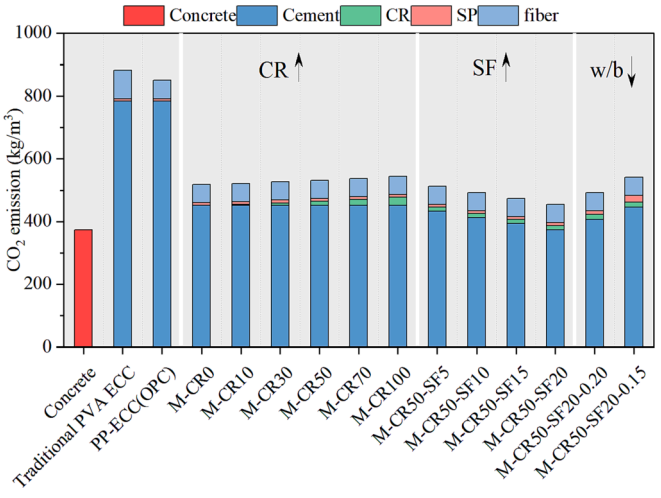

Fig. 15. Carbon emission of all mixtures.

matrix and stretched, providing particle bridges that transfer load and restrain crack opening. This particle bridging effect was also identified by Segre et al. in conventional concrete [54]. Also, some microcracks could be initiated by CR particles since CR particles are soft and hydrophobic and can behave like voids, then followed by crack bridging by CR particles. This is beneficial for tight crack width due to the superposition curve of fiber bridging and rubber particle bridging as shown in Fig. 12(c), where the slope of the σ-δ curve is increased and the crack opening δ is reduced at a given cracking stress.

Similarly, the mechanism of silica fume and w/b ratio can also be explained by the stress-crack opening (σ-δ) relation. High pozzolanic reactivity and the pore-filling effect of silica fume as well as the reduced porosity by low w/b ratio densified the matrix, resulting in higher cracking stress and enlarged crack width. Besides, the densification of the fiber/matrix interface enhanced the interfacial bonding of fiber/matrix and induced a steeper curve slope, and reduced the crack width opposite to that shown in Fig. 12(b). The coupled effect of these above mechanisms leads to the observed increase in crack width in these mixtures containing SF or with lower w/b ratios.

4. Environmental and economic impacts

To evaluate the environmental and economic impact of the studied ECC mixtures, Material Sustainability Indices (MSIs) were calculated to quantitatively represent the material greenness involved in the production process. The energy consumption, carbon emission, and the cost on a unit weight basis of each mixture ingredient are collected from literature, database, and local contractors and shown in Table 5. These parameters are calculated based on the industrial and the best available technology level with life cycle assessment (LCA) and are widely used by databases and research publications. For example, the MSIs of cement capture the total energy consumption and carbon emission along the whole production chain, including raw materials extraction, fuel extraction, the transport of raw materials and fuels, the clinkerization as well as the calcination of clays for the LC3 case, the grinding, packing and other processes [55]. The MSIs of the LC3 binder are lower than that of OPC due to the reduced proportion of clinker as shown in Table 5. Since FA and SF are industrial wastes, negligible energy intensity and carbon emissions are assumed in this study. While CR is produced from waste rubber tires, the production of CR involved in the grinding process accounts for the energy consumption and carbon emissions. The energy intensity and carbon emissions of fibers are also calculated on a cradle-to-gate basis including feedstock production, transportation, distribution, and process conversion.

Based on the parameters of each ingredient, the embodied energy and carbon emissions of all mixtures are calculated and shown in Fig. 14 and Fig. 15, respectively, and the information on conventional concrete [13,56], traditional PVA-ECC, and PP-OPC based ECC with the same mixture design as M−CR0 is also included for comparison. The embodied energy and carbon emission of traditional PVA-ECC are 2.9 and 2.4 times that of conventional concrete, respectively. This stems from the high volume of cement in ECC mixture design due to the lack of coarse aggregate and the high energy consumption and carbon emission of fiber. Besides, the PP-OPC-based ECC still has high carbon emissions but lower embodied energy caused by the larger embodied energy difference between these two types of fiber. When OPC and PVA fiber are replaced by LC3 and PP fiber, the embodied energy and carbon emission of ECC are reduced by 31 % and 41 %, respectively. FA is a direct industrial byproduct with negligible embodied energy and carbon emissions, while crumb rubber manufacturing involves energy consumption and carbon emission associated with the grinding process. Hence, both the embodied energy and carbon emissions increase with FA substitution by CR. Similarly, with negligible embodied energy and carbon

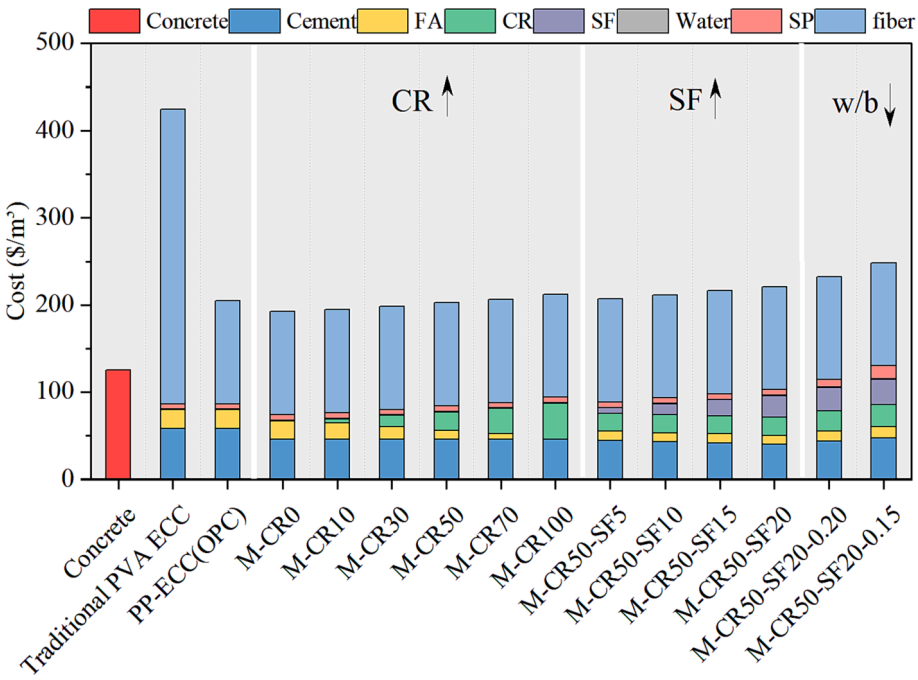

Fig. 16. Estimated cost of all mixtures.

emission [15], partial replacement of cement by silica fume leads to the reduction of embodied energy and carbon emission highly by 8.1 % and 14.6 %, respectively. Lowering the w/b ratio means more raw ingredients except for water in the unit volume of ECC composite, resulting in higher embodied energy and carbon emission. Compared to the w/b ratio of 0.25, the w/b ratio of 0.15 possesses 18.2 % and 19.2 % higher embodied energy and carbon emissions.

The estimated cost of all mixtures is shown in Fig. 16. The cost of the traditional PVA-ECC is 3.4 times that of conventional concrete since PVA fiber takes up 80 % of the total cost. With the cost-effective PP fiber, the total cost is reduced significantly by 52 %. The use of LC3 further lowers the cost, while the relatively high price of CR increases the cost slightly due to the low density and low mass dosage of CR in the mixture composition. Similarly, incorporating silica fume and lowering w/b ratio further increase the cost by 12.6 %. Overall, the mixture M−CR70 exhibits the tight crack width control ability, which is comparable to that of PVA-ECC, and also reduces the embodied energy, carbon emission, and cost by 25.9 %, 39.2 %, and 51.4 %, respectively.

With a tight crack width of about 50 μm at 1 % strain (considered large for real-world applications), M−CR70 is expected to have extreme durability based on extensive data sets as discussed in [1]. In this manner, it may be anticipated that operational carbon associated with infrequent repair events of civil infrastructure will be low compared to those built with conventional concrete. Additional studies on durability performance of M−CR70 and life cycle analysis for specific infrastructure applications will be required to quantify such expectations, beyond the scope of the present study.

5. Conclusions

The objective of this research is to develop a ductile ECC with reduced embodied carbon and energy compared to traditional ECC (with OPC binder and reinforced with PVA fiber), and with microcrack width controlled to around 50 μm. Tight crack width is necessary for durable infrastructure requiring minimum repair needs and hence reduced operational carbon footprint. Based on the experimental findings, the following can be concluded:

An ECC composed of greener polypropylene (PP) fiber and limestone calcined clay cement (LC3) binder has been successfully designed and tested. The developed PP-ECC possesses a tensile strength of 2.24–3.82 MPa and tensile strain capacity of 2.42–10.39 %. Tight crack width down to about 50 μm at 1 % tensile strain was attained.

The control of crack width using crumb rubber particles has been experimentally confirmed. Increasing the replacement of fly ash by crumb rubber leads to a continuous drop in crack width, however, at the expense of loss of compressive strength. An optimal replacement content is around 50 %. At this level, a 28-day compressive strength of 22 MPa can be retained. Partial restoration of compressive strength can be attained with the use of silica fume and reduced w/binder ratio.

The resulting PP-ECC has lower carbon and energy footprint compared with traditional PVA-ECC. The embodied energy, carbon emission, and cost of the PP-ECC were reduced by 21.1 %–33.2 %, 38.2 %-48.6 %, and 41.5 %-54.7 %, respectively. Combined with the intrinsically tight crack width, the developed PP-ECC can contribute to sustainable infrastructure with lower embodied and operational carbon.

Considering the mechanical properties, crack width control, as well as economic and environmental impact, the ideal mix composition is found to be 50 %-70 % CR content with low SF content(~5%).

While the developed PP-ECC possesses good ductility and well-controlled tight crack width, this composite shows limited compressive strength due to the use of crumb rubber particles. Additional research is needed to address this shortcoming. The expected improvement in durability under various environmental exposures requires experimental verification in future studies. Finally, the underlying mechanisms of crack control by crumb rubber particles warrant further investigations.

CRediT authorship contribution statement

Mengjun Hou: Methodology, Investigation, Validation, Writing – original draft. **Duo Zhang:** Supervision, Writing – review & editing. **Victor C. Li:** Conceptualization, Supervision, Validation, Writing – review & editing.

Declaration of Competing Interest

The authors declare that they have no known competing financial interests or personal relationships that could have appeared to influence

the work reported in this paper.

Data availability

Data will be made available on request.

Acknowledgment

This research is financially supported by ARPA-e funding (No. DE-AR0001141) from the US Department of Energy to the University of Michigan. Materials supply from Boral Resources (fly ash), BASF (superplasticizer) is gratefully acknowledged.

References

[1] V.C. Li, Engineered cementitious composites (ECC): bendable concrete for sustainable and resilient infrastructure, Springer, Berlin Heidelberg (2019), https://doi.org/10.1007/978-3-662-58438-5.
[2] V.C. Li, S. Wang, C. Wu, Tensile strain-hardening behavior or polyvinyl alcohol engineered cementitious composite (PVA-ECC), ACI Mater, J 98 (2001) 483–492, https://doi.org/10.14359/10851.
[3] H. Ma, C. Yi, C. Wu, Review and outlook on durability of engineered cementitious composite (ECC), Constr. Build. Mater. 287 (2021), https://doi.org/10.1016/j.conbuildmat.2021.122719.
[4] H. Liu, Q. Zhang, V. Li, H. Su, C. Gu, Durability study on engineered cementitious composites (ECC) under sulfate and chloride environment, Constr. Build. Mater. 133 (2017) 171–181, https://doi.org/10.1016/j.conbuildmat.2016.12.074.
[5] M. Şahmaran, V.C. Li, Durability of mechanically loaded engineered cementitious composites under highly alkaline environments, Cem. Concr. Compos. 30 (2008) 72–81, https://doi.org/10.1016/j.cemconcomp.2007.09.004.
[6] M. Şahmaran, V.C. Li, Durability properties of micro-cracked ECC containing high volumes fly ash, Cem. Concr. Res. 39 (2009) 1033–1043, https://doi.org/10.1016/j.cemconres.2009.07.009.
[7] E.H. Yang, V.C. Li, Strain-hardening fiber cement optimization and component tailoring by means of a micromechanical model, Constr. Build. Mater. 24 (2010) 130–139, https://doi.org/10.1016/j.conbuildmat.2007.05.014.
[8] Q. Jin, V.C. Li, Development of lightweight engineered cementitious composite for durability enhancement of tall concrete wind towers, Cem. Concr. Compos. 96 (2019) 87–94, https://doi.org/10.1016/j.cemconcomp.2018.11.016.
[9] B. Felekoglu, K. Tosun-Felekoglu, R. Ranade, Q. Zhang, V.C. Li, Influence of matrix flowability, fiber mixing procedure, and curing conditions on the mechanical performance of HTPP-ECC, Compos. Part B Eng. 60 (2014) 359–370, https://doi.org/10.1016/j.compositesb.2013.12.076.
[10] K. Tosun-Felekoğlu, E. Gödek, M. Keskinateş, B. Felekoğlu, Utilization and selection of proper fly ash in cost effective green HTPP-ECC design, J. Clean. Prod. 149 (2017) 557–568, https://doi.org/10.1016/j.jclepro.2017.02.117.
[11] M. Singh, B. Saini, H.D. Chalak, Performance and composition analysis of engineered cementitious composite (ECC) – A review, J. Build. Eng. 26 (2019), 100851, https://doi.org/10.1016/j.jobe.2019.100851.
[12] D. Shoji, Z. He, D. Zhang, V.C. Li, The Greening of Engineered Cementitious Composites (ECC): A Review, Constr. Build. Mater. 327 (2022) 1–19, https://doi.org/10.1016/j.conbuildmat.2022.126701.
[13] E.H. Yang, Y. Yang, V.C. Li, Use of high volumes of fly ash to improve ECC mechanical properties and material greenness, ACI Mater. J. 104 (2007) 620–628, https://doi.org/10.14359/18966.
[14] C. Yoganantham, P.S. Joanna, Effect of high volume fly ash concrete in self-curing engineered cementitious composite (ECC), Int. J. Adv. Res. Eng. Technol. 11 (2020) 268–276, https://doi.org/10.34218/IJARET.11.4.2020.027.
[15] J. Yu, C.K.Y. Leung, Strength Improvement of Strain-Hardening Cementitious Composites with Ultrahigh-Volume Fly Ash, J. Mater. Civ. Eng. 29 (2017) 05017003, https://doi.org/10.1061/(asce)mt.1943-5533.0001987.
[16] Z. Pan, X. Zeng, Z. Hu, Effect of Fly Ash and Silica Fume on Mechanical Properties of High-Performance FRCC, IOP Conf. Ser. Mater. Sci. Eng. 562 (1) (2019) 012048.
[17] H. Ma, S. Qian, V.C. Li, Influence of fly ash type on mechanical properties and self-healing behavior of Engineered Cementitious Composite (ECC), 9th Int. Conf. Fract. Mech. Concr. Concr. Struct., 9th International Conference on Fracture Mechanics of Concrete and Concrete Structures (2016), https://doi.org/10.21012/fc9.209.
[18] L. Kan, R. Shi, J. Zhu, Effect of fineness and calcium content of fly ash on the mechanical properties of Engineered Cementitious Composites (ECC), Constr. Build. Mater. 209 (2019) 476–484.
[19] K. Scrivener, F. Martirena, S. Bishnoi, S. Maity, Calcined clay limestone cements (LC3), Cem. Concr. Res. 114 (2018) 49–56, https://doi.org/10.1016/j.cemconres.2017.08.017.
[20] D. Zhang, B. Jaworska, H. Zhu, K. Dahlquist, V.C. Li, Engineered Cementitious Composites (ECC) with limestone calcined clay cement (LC3), Cem. Concr. Compos. 114 (2020), 103766, https://doi.org/10.1016/j.cemconcomp.2020.103766.
[21] H. Zhu, D. Zhang, T. Wang, H. Wu, V.C. Li, Mechanical and self-healing behavior of low carbon engineered cementitious composites reinforced with PP-fibers, Constr. Build. Mater. 259 (2020), 119805, https://doi.org/10.1016/j.conbuildmat.2020.119805.
[22] L. Wang, N. Ur, I. Curosu, Z. Zhu, M. Abdul, B. Beigh, M. Liebscher, L. Chen, D.C. W. Tsang, S. Hempel, V. Mechtcherine, Cement and Concrete Research On the use of limestone calcined clay cement (LC 3) in high-strength strain-hardening cement-based composites (HS-SHCC), Cem. Concr. Res. 144 (2021) 1–13.
[23] Z. Zhang, A. Yuvaraj, J. Di, S. Qian, Matrix design of light weight, high strength, high ductility ECC, Constr. Build. Mater. 210 (2019) 188–197, https://doi.org/10.1016/j.conbuildmat.2019.03.159.
[24] Y. Liu, X. Zhou, C. Lv, Y. Yang, T. Liu, Use of Silica Fume and GGBS to Improve Frost Resistance of ECC with High-Volume Fly Ash, Adv. Civ. Eng. 2018 (2018), https://doi.org/10.1155/2018/7987589.
[25] T. Kanda, Design of engineered cementitious composites for ductile seismic resistant elements, University of Michigan, 1998.
[26] V.C. Li, Tailoring ECC for Special Attributes: A Review, Int. J. Concr. Struct. Mater. 6 (2012) 135–144, https://doi.org/10.1007/s40069-012-0018-8.
[27] S. Wang, V.C. Li, Tailoring of pre-existing flaws in ECC matrix for saturated strain hardening, Framcos 2004 (2004) 1005–1012.
[28] Y. Zhou, B. Xi, L. Sui, S. Zheng, F. Xing, L. Li, Development of high strain-hardening lightweight engineered cementitious composites : Design and performance 104 (2019), https://doi.org/10.1016/j.cemconcomp.2019.103370.
[29] K. Yu, H. Zhu, M. Hou, V.C. Li, Self-healing of PE-fiber reinforced lightweight high-strength engineered cementitious composite, Cem. Concr. Compos. 123 (2021), 104209, https://doi.org/10.1016/j.cemconcomp.2021.104209.
[30] I. Abdulkadir, B.S. Mohammed, M.S. Liew, M. Mubarak, B. Abdul, N. Amila, W. Abdullah, S. As, A review of the effect of waste tire rubber on the properties of ECC International Journal of Advanced and Applied Sciences A review of the effect of waste tire rubber on the properties of, ECC (2021), https://doi.org/10.21833/ijaas.2020.08.011.
[31] H. Ma, S. Qian, Z. Zhang, Z. Lin, V.C. Li, Tailoring Engineered Cementitious Composites with local ingredients, Constr. Build. Mater. 101 (2015) 584–595, https://doi.org/10.1016/j.conbuildmat.2015.10.146.
[32] Z. Zhang, H. Ma, S. Qian, Investigation on properties of ECC incorporating crumb rubber of different sizes, J. Adv. Concr. Technol. 13 (2015) 241–251, https://doi.org/10.3151/jact.13.241.
[33] Y. Wang, Z. Zhang, J. Yu, J. Xiao, Q. Xu, Using green supplementary materials to achieve more ductile ECC, Materials (Basel). 12 (6) (2019) 858.
[34] A. Adesina, S. Das, Performance of engineered cementitious composites incorporating crumb rubber as aggregate, Constr. Build. Mater. 274 (2021), 122033, https://doi.org/10.1016/j.conbuildmat.2020.122033.
[35] Z. Zhang, F. Qin, H. Ma, L. Xu, Tailoring an impact resistant engineered cementitious composite (ECC) by incorporation of crumb rubber, Constr. Build. Mater. 262 (2020), 120116, https://doi.org/10.1016/j.conbuildmat.2020.120116.
[36] E. Güneyisi, M. Gesoğlu, T. Özturan, Properties of rubberized concretes containing silica fume, Cem. Concr. Res. 34 (12) (2004) 2309–2317.
[37] T. Gupta, S. Chaudhary, R.K. Sharma, Mechanical and durability properties of waste rubber fiber concrete with and without silica fume, J. Clean. Prod. 112 (2016) 702–711, https://doi.org/10.1016/j.jclepro.2015.07.081.
[38] D. Zhang, H.e. Zhu, M. Hou, K.E. Kurtis, P.J.M. Monteiro, V.C. Li, Optimization of matrix viscosity improves polypropylene fiber dispersion and properties of engineered cementitious composites, Constr. Build. Mater. 346 (2022) 128459.
[39] Jsce, Recommendations for design and construction of high performance fiber reinforced cement composites with multiple fine cracks, Japan Soc, Civ. Eng. (2008).
[40] M. Xu, J. Yu, J. Zhou, Y. Bao, V.C. Li, Effect of curing relative humidity on mechanical properties of engineered cementitious composites at multiple scales, Constr. Build. Mater. 284 (2021), 122834, https://doi.org/10.1016/j.conbuildmat.2021.122834.
[41] A. Katz, V.C. Li, A special technique for determining the bond strength of micro-fibres in cement matrix by pullout test, J. Mater. Sci. Lett. 15 (1996) 1821–1823, https://doi.org/10.1007/BF00275353.
[42] C. Redon, V.C. Li, C. Wu, H. Hoshiro, T. Saito, A. Ogawa, Measuring and modifying interface properties of PVA fibers in ECC matrix, J. Mater. Civ. Eng. 13 (6) (2001) 399–406.
[43] Astm, C109, ASTM C109 / C109M–20b. Standard Test Method for Compressive Strength of Hydraulic Cement Mortars (Using 2-in. or [50 mm], Cube Specimens), Annu. B. ASTM Stand. 04 (2016) 9.
[44] ASCE, Standard Test Method for Linear-Elastic Plane-Strain Fracture Toughness KIc of Metallic Materials, E399. (2019), ASCE (2019) 1–35, https://doi.org/10.1520/E0399-09E02.2.
[45] V.C. Li, D.K. Mishra, H.C. Wu, Matrix design for pseudo-strain-hardening fibre reinforced cementitious composites, Mater. Struct. 28 (1995) 586–595, https://doi.org/10.1007/BF02473191.
[46] A. Al-Fakih, B.S. Mohammed, M.S. Liew, On rubberized engineered cementitious composites (R-ECC): A review of the constituent material, Case Stud. Constr. Mater. 14 (2021).
[47] X. Sun, S. Wu, J. Yang, R. Yang, Mechanical properties and crack resistance of crumb rubber modified cement-stabilized macadam, Constr. Build. Mater. 259 (2020), 119708, https://doi.org/10.1016/j.conbuildmat.2020.119708.
[48] M.I. Khan, R. Siddique, Utilization of silica fume in concrete: Review of durability properties, Resour. Conserv. Recycl. 57 (2011) 30–35, https://doi.org/10.1016/j.resconrec.2011.09.016.
[49] G. Prokopski, B. Langier, Effect of water/cement ratio and silica fume addition on the fracture toughness and morphology of fractured surfaces of gravel concretes, Cem. Concr. Res. 30 (2000) 1427–1433, https://doi.org/10.1016/S0008-8846(00)00332-X.
[50] B.B. Sabir, Strength and fracture toughness of silica fume concrete, Mag. Concr. Res. 48 (1997) 139–146, https://doi.org/10.1680/macr.1997.49.179.139.

[51] S. Zhang, V.C. Li, G. Ye, Micromechanics-guided development of a slag/fly ash-based strain-hardening geopolymer composite, Cem. Concr. Compos. 109 (2020), 103510, https://doi.org/10.1016/j.cemconcomp.2020.103510.
[52] J. Feng, F. Yang, S. Qian, Improving the bond between polypropylene fiber and cement matrix by nano calcium carbonate modification, Constr. Build. Mater. 269 (2021), 121249, https://doi.org/10.1016/j.conbuildmat.2020.121249.
[53] S. He, S. Zhang, M. Luković, E. Schlangen, Effects of bacteria-embedded polylactic acid (PLA) capsules on fracture properties of strain hardening cementitious composite (SHCC), Eng. Fract. Mech. 268 (2022), 108480, https://doi.org/10.1016/j.engfracmech.2022.108480.
[54] N. Segre, C. Ostertag, P.J.M. Monteiro, Effect of tire rubber particles on crack propagation in cement paste, Mater. Res. 9 (2006) 311–320, https://doi.org/10.1590/S1516-14392006000300011.
[55] S. Sánchez Berriel, A. Favier, E. Rosa Domínguez, I.R. Sánchez MacHado, U. Heierli, K. Scrivener, F. Martirena Hernández, G. Habert, Assessing the environmental and economic potential of Limestone Calcined Clay Cement in Cuba, J. Clean. Prod. 124 (2016) 361–369, https://doi.org/10.1016/j.jclepro.2016.02.125.
[56] Concretenetwork.com, CONCRETE PRICE CONSIDERATIONS - COST OF CONCRETE, (n.d.). https://www.concretenetwork.com/concrete-prices.html.
[57] A.P. Fantilli, B. Chiaia, A. Gorino, Ecological and mechanical assessment of lightweight fiber-reinforced concrete made with rubber or expanded clay aggregates, Constr. Build. Mater. 127 (2016) 692–701, https://doi.org/10.1016/j.conbuildmat.2016.10.020.
[58] M. Chen, H. Zhong, L. Chen, Y. Zhang, M. Zhang, Engineering properties and sustainability assessment of recycled fibre reinforced rubberised cementitious composite, J. Clean. Prod. 278 (2021), 123996, https://doi.org/10.1016/j.jclepro.2020.123996.
[59] H.L. Wu, D. Zhang, B.R. Ellis, V.C. Li, Development of reactive MgO-based Engineered Cementitious Composite (ECC) through accelerated carbonation curing, Constr. Build. Mater. 191 (2018) 23–31, https://doi.org/10.1016/j.conbuildmat.2018.09.196.
[60] Granta (CES) EduPack, Cambridge, UK, 2021, (n.d.).